Science of the Total Environment 628–629 (2018) 611–620

Contents lists available at ScienceDirect

Science of the Total Environment

journal homepage: www.elsevier.com/locate/scitotenv

Global patterns of extreme drought-induced loss in land primary production: Identifying ecological extremes from rain-use efficiency

Ling Du [a], Nathaniel Mikle [a,b], Zhenhua Zou [a], Yuanyuan Huang [a,c], Zheng Shi [a], Lifen Jiang [a,1], Heather R. McCarthy [a], Junyi Liang [a,d], Yiqi Luo [a,e,1,*]

[a] Department of Microbiology and Plant Biology, University of Oklahoma, Norman, OK 73019, USA
[b] US Geological Survey, Northern Rocky Mountain Science Center, West Glacier, MT 59936, USA
[c] Laboratoire des Sciences du Climat et de l'Environnement, CEA-CNRS-UVSQ, 91191 Gif sur Yvette, France
[d] Environmental Sciences Division & Climate Change Science Institute, Oak Ridge National Laboratory, Oak Ridge, TN 37830, USA
[e] Department of Earth System Science, Tsinghua University, Beijing 100084, China

HIGHLIGHTS

- A novel method was developed to detect extreme drought-induced loss of ecosystem function globally.
- Large well-known extreme drought events were detected mainly in semi-arid regions.
- GPP reduction caused by functional loss could explain ≥70% of the interannual variation in GPP in drought-affected areas.

GRAPHICAL ABSTRACT

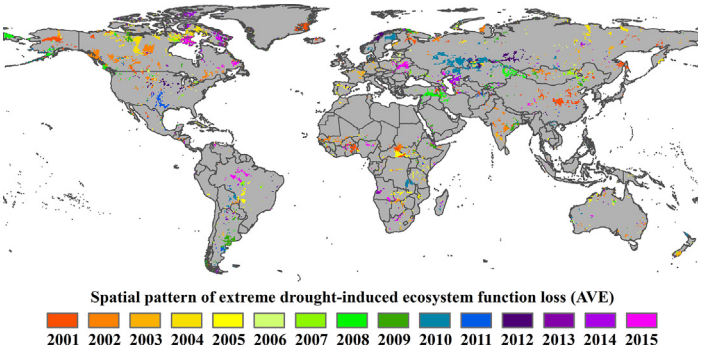

ARTICLE INFO

Article history:
Received 17 October 2017
Received in revised form 9 February 2018
Accepted 10 February 2018
Available online 20 February 2018

Editor: Elena Paoletti

Keywords:
Extreme drought
Ecosystem function
Rain-use efficiency
GPP
Semi-arid regions
Interannual variation

ABSTRACT

Quantifying the ecological patterns of loss of ecosystem function in extreme drought is important to understand the carbon exchange between the land and atmosphere. Rain-use efficiency [RUE; gross primary production (GPP)/precipitation] acts as a typical indicator of ecosystem function. In this study, a novel method based on maximum rain-use efficiency (RUE_{max}) was developed to detect losses of ecosystem function globally. Three global GPP datasets from the MODIS remote sensing data (MOD17), ground upscaling FLUXNET observations (MPI-BGC), and process-based model simulations (BESS), and a global gridded precipitation product (CRU) were used to develop annual global RUE datasets for 2001–2011. Large, well-known extreme drought events were detected, e.g. 2003 drought in Europe, 2002 and 2011 drought in the U.S., and 2010 drought in Russia. Our results show that extreme drought-induced loss of ecosystem function could impact 0.9% ± 0.1% of earth's vegetated land per year and was mainly distributed in semi-arid regions. The reduced carbon uptake caused by functional loss (0.14 ± 0.03 PgC/yr) could explain >70% of the interannual variation in GPP in drought-affected areas ($p \leq 0.001$). Our results highlight the impact of ecosystem function loss in semi-arid regions with increasing precipitation variability and dry land expansion expected in the future.

* Corresponding author at: Center for Ecosystem Science and Society, Northern Arizona University, Flagstaff, AZ 86011, USA.
E-mail address: yiqi.luo@nau.edu (Y. Luo).
[1] Current address: Center for Ecosystem Science and Society, Northern Arizona University, Flagstaff, Arizona 86011, USA.

https://doi.org/10.1016/j.scitotenv.2018.02.114
0048-9697/

1. Introduction

Climate change is projected to increase the frequency and intensity of drought in the mid- to late 21st century (Stocker et al., 2013). Droughts can alter the terrestrial carbon cycle by affecting the composition, structure and functioning of ecosystems. Under extreme climate conditions, enhanced droughts and heat waves could fundamentally alter the structure or function of terrestrial ecosystems, outside the bounds of what is typical or normal variability (Smith, 2011; Reichstein et al., 2013). Currently, the methods to investigate extreme ecological responses to extreme climate events, as well as the mechanisms and processes determining ecosystem responses are still lacking (Smith, 2011). Thus, quantifying the spatiotemporal patterns of ecological responses to extreme drought is critical to predict future drought impacts under climate change.

Ecological responses to droughts has been observed variable ranging from little ecosystem impacts to major alteration of ecosystem structure and function (Smith, 2011). The ability of an ecosystem to maintain its normal function during droughts greatly relies on the resistance of the ecosystem to environmental stresses, which is fundamentally determined by processes of drought tolerance and functionality of plant communities and the availability of water in the ecosystem (Mariotte et al., 2013). Extreme drought-induced loss of ecosystem function may occur when drought-resistant measures utilized by plant communities (e.g. closure of stomata, favoring drought-resistant plants) become overwhelmed by plant hydraulic limitations or mortality with further stress (Reyer et al., 2013). Loss of ecosystem function during extreme drought could cause an ecosystem to shift from carbon sink to carbon source, which can strongly influence the carbon exchange between the land and atmosphere (Frank et al., 2015).

At the beginning of the 21st century, large-scale, extreme droughts have occurred throughout the world, attracting the attention of scientists (Breshears et al., 2005; Ciais et al., 2005; Schwalm et al., 2012; Doughty et al., 2015). Many studies have examined the regional or global impacts of droughts on terrestrial ecosystems and the carbon cycle by identifying drought events from a meteorological perspective (Ciais et al., 2005; Zhao and Running, 2010; Schwalm et al., 2012; Huang et al., 2016). In these studies, droughts were usually identified by climate variables or other environmental drivers (e.g. precipitation, drought indices). There have also been some efforts to quantify the spatiotemporal ecological extremes using statistical techniques (Liu et al., 2013; Hoover et al., 2014; Zscheischler et al., 2014). Extreme ecological responses were identified by classifying the deviation of ecosystem variables (e.g. GPP, NDVI) from the norms derived from long-term datasets. A wide range of ecosystem responses to drought has been identified, from little impact on vegetation function in some instances, to major reductions in primary production in others (Ciais et al., 2005; Zhao and Running, 2010; Jentsch et al., 2011; Zscheischler et al., 2014). However, integrating ecological processes of how ecosystems functionally respond to extreme droughts have not been broadly considered in identifying drought impacts. Thus, the patterns of extreme ecological responses to droughts have not been well quantified globally from the ecological perspective.

On a global scale, it is widely reported that severe droughts caused by precipitation reduction can induce extensive plant mortality and an associated reduction in productivity (Allen et al., 2010; Peng et al., 2011; Doughty et al., 2015). How ecosystems respond to greater precipitation variability is a new frontier for ecologists (Knapp et al., 2017; Luo et al., 2017). Generally, ecosystems are composed of plant communities that have adapted to current water conditions to be fully functional under a wide range of conditions. Thus, ecosystems can withstand the effects of moderate water shortage and sustain productivity by increasing plant water-use efficiency through the closure of stomata or favoring high water-use efficiency species, and less water is lost through runoff and evaporation (Mariotte et al., 2013; Ponce Campos et al., 2013). However, when water shortage becomes more severe (i.e. extreme drought), more water could be lost through evaporation resulting from increasing ratio between evaporation and carbon uptake or plant mortalities due to carbon starvation or hydraulic failure) (McDowell et al., 2008; Choat et al., 2012). Thus, loss of ecosystem function could occur when the plant communities are not able to use the existing water resources to maintain resistance (e.g. increasing water-use efficiency) during extreme drought. And there must exist thresholds at which ecosystems function turns to decline in extreme drought, which is still largely unknown and has great scientific significance (Estiarte et al., 2016).

Here, we developed a new method to detect the extreme drought-induced loss of ecosystem function globally from an ecological perspective. In this study, rain-use efficiency (RUE; GPP/precipitation) was utilized as the typical indicator of ecosystem function. We assumed that RUE increases with decreasing precipitation to a maximum (RUE_{max}) during moderate drought (Huxman et al., 2004; Ponce Campos et al., 2013), and that RUE will decline when water shortage is beyond the tolerance of current vegetation, leading to loss of ecosystem function. The main objective of this study was to detect the ecological patterns of extreme drought-induced loss of ecosystem function globally for the beginning of this century (2001−2011) and understand its implications for the carbon cycle. Three global GPP datasets were used to establish three RUE datasets and each RUE dataset was used to detect loss of ecosystem function individually. The spatiotemporal extent of ecosystem function loss and its impact on the terrestrial carbon cycle were further analyzed in this study.

2. Materials and methods

2.1. Data sources

We used three different GPP datasets and a precipitation dataset to establish three global RUE datasets. All datasets used are listed in Table 1.

The MODIS GPP product (MOD17.055) was produced by the Numerical Terradynamic Simulation Group (NTSG)/University of Montana (UMT) (http://www.ntsg.umt.edu/project/mod17). It provides monthly GPP data with a 0.05° spatial resolution for the period 2000–2015 (Zhao and Running, 2010). This product was developed from production efficiency model using MODIS vegetation indices and meteorological information as inputs. Its accuracy has been independently assessed for scientific research and it is a primary data source used to evaluate the spatial distribution and long term trend of vegetation productivity (Anav et al., 2015).

The BESS GPP product was generated from a simplified process-based model (Breathing Earth System Simulator) which couples atmosphere and canopy radiative transfers, photosynthesis, evapotranspiration, and energy balance (Jiang and Ryu, 2016). It provides monthly GPP data at 0.5° spatial resolution from 2001 to 2015 (http://environment.snu.ac.kr/bess/). This new process model-based GPP product serves as a dataset independent from remote sensing and ground observations.

The MPI-BGC GPP product from the Max Planck Institute for Biogeochemistry were up-scaled from ground FLUXNET observations of CO_2, water, and energy fluxes to global scale using the model tree ensemble (MTE) technique (Jung et al., 2011). The MTE model was first trained to predict site-level GPP based on remote sensing indices and meteorological data, and then it was applied globally to generate GPP at a 0.5° spatial resolution and a monthly temporal resolution from 1982 to 2011 (http://www.bgc-jena.mpg.de/geodb/). As a proxy for FLUXNET observations, this empirically derived GPP product has been commonly considered as the benchmark or reference for calibration and evaluation of other model results (Piao et al., 2013; Anav et al., 2015). Nevertheless, large uncertainties still exist in the regions with few observation stations (e.g. South America, Africa).

Table 1
Datasets used in this study.

Variable	Description	Temporal resolution	Spatial resolution	Reference
MODIS GPP	Gross primary productivity derived from MODIS (MOD17.055) remote sensing observations	Monthly 2000–2015	0.05°	(Zhao and Running, 2010)
BESS GPP	Gross primary productivity derived from process-based model	Monthly 2001–2015	0.5°	(Jiang and Ryu, 2016)
MPI-BGC GPP	Gross primary productivity derived from ground FLUXNET observations	Monthly 1982–2011	0.5°	(Jung et al., 2011)
CRU PRE	Precipitation from CRU TS 3.24.01 (Climatic Research Unit at the University of East Anglia)	Monthly 1901–2015	0.5°	(Harris et al., 2014)

The global gridded precipitation dataset used in this study was from Climate Research Unit (CRU), version TS 3.24.01 (Harris et al., 2014). It provides monthly precipitation at 0.5° spatial resolution spanning from 1901 to 2015 (https://crudata.uea.ac.uk/cru/data/hrg/). The global precipitation dataset is based on analysis of >4000 individual meteorological station records and spatially interpolated using autocorrelation functions. This precipitation product has been widely evaluated and used in global change studies (de Jong et al., 2013; Wu et al., 2015).

2.2. Rain-use efficiency datasets

In our study, the common time period of the three GPP datasets (2001–2011) was chosen as the study period. The MODIS GPP product were aggregated to a 0.5° spatial resolution to match the other two GPP datasets. The monthly data of all three GPP datasets were respectively summed annually to estimate the annual GPP datasets. In order to match the three GPP datasets, monthly precipitation data were also summed annually for 2001–2011.

Based on the definition of rain-use efficiency (productivity per unit of precipitation, $gC/m^2/mm$), three annual GPP datasets were divided by the annual precipitation dataset to generate three global RUE datasets (MODIS RUE, BESS RUE, and MPI-BGC RUE) at 0.5° spatial resolution during 2001–2011. Due to the longer-time data availability of MODIS GPP and BESS GPP, we also generated an annual average RUE dataset (AVE RUE) for 2001–2015 using the average of MODIS GPP and BESS GPP for longer term analysis.

2.3. Detecting ecosystem function loss

For each RUE dataset during 2001–2011, the detection of ecosystem function loss was implemented pixel by pixel globally based on the relationship between RUE and precipitation. For each pixel, we assumed that the RUE of an ecosystem increases gradually to a maximum (RUE_{max}) as precipitation decreases, and then declines when the water shortage exceeds the plant community tolerance (ecosystem resistance) to the extent that ecosystem function declines. To characterize ecosystem responses to extreme drought, we first identified RUE_{max} during the study period. Numerically, we identified the greatest value of the 11-year RUE estimates as the RUE_{max}. Then, the precipitation at RUE_{max} was selected as a threshold at which abrupt changes in ecosystem function could occur with further precipitation reductions. Using this threshold, each RUE dataset was separated into two parts at the pixel level: 1) Data with precipitation at or above the threshold for normal years; and 2) data with precipitation below the threshold for possible drought years. For the data points in normal years, the precipitation and corresponding RUE estimates were used to build a linear regression model (Fig. 1). The regression model was further extended to data points below the precipitation threshold in drought years with 95% confidence bound. If the data points during drought years were below the lower 95% confidence bound of the regression (the lower limit of ecosystem variability), loss of ecosystem function had occurred (Fig. 1). This algorithm was applied to obtain the global spatial patterns of ecosystem function loss for 2001–2011 and 2001–2015, respectively.

In this study, only the pixels with >6 data points (8 data points for 2001–2015) in normal years were selected to build the linear regression model, since this represents the majority of years in the study period (Fig. S1). Furthermore, only the pixels with statistically significant regressions between RUE and precipitation ($p < 0.05$) were used to identify ecosystem function loss (Fig. S1 and Fig. S2). Overall, >85%, 91%, and 82% of the earth vegetated land surface, respectively, in MODIS RUE, BESS RUE, and MPI-BGC RUE datasets showed significant correlations between RUE and precipitation. Thus, >80% of the vegetated land was available to analyze the global patterns of extreme drought-induced ecosystem function loss.

2.4. Estimation of GPP reduction and its spatiotemporal variation

In this study, for each pixel, the years with ecosystem function losses were detected and recorded based on the method shown in Fig. 1. Using the average of GPP values in non-drought years as the baseline, the GPP reduction due to ecosystem function loss in each pixel was calculated as the difference of the GPP value of current drought year and the baseline. Through the spatial integration of GPP reduction pixel by pixel, annual regional and global GPP reductions could be estimated. To evaluate the impact of ecosystem function loss on the terrestrial carbon cycle, the GPP reduction was then compared with the GPP anomaly in drought-affected areas. Additionally, we also estimated the GPP reductions across biomes to analyze the extreme drought impacts on different terrestrial ecosystems.

3. Results

3.1. Precipitation threshold of ecosystem function loss based on RUE_{max}

The precipitation at RUE_{max} was selected as the threshold at which abrupt alteration of ecosystem function could occur with further water shortage. In each pixel, the greatest value of RUE estimates (RUE_{max}) was first identified during 2001–2011 and then the precipitation at the RUE_{max} was recorded as the threshold. The spatial distributions of the precipitation threshold in 2001–2011 were extracted based on three RUE datasets respectively (Fig. 2). The general patterns of the precipitation threshold were similar in all three RUE datasets. For example, the precipitation thresholds at the forest site in Europe (3.54° N, 46.48°E) were identified as 673.4 mm in three datasets, and the precipitation thresholds at the grassland site in southern U.S. (36.23°N, 98.74°W) were identified 469.1 mm in three datasets (Fig. 1).

At the global scale, the distribution of the precipitation threshold follows a latitudinal gradient. It decreases from low latitude to high latitude and from wet areas to dry areas. In addition, the spatial

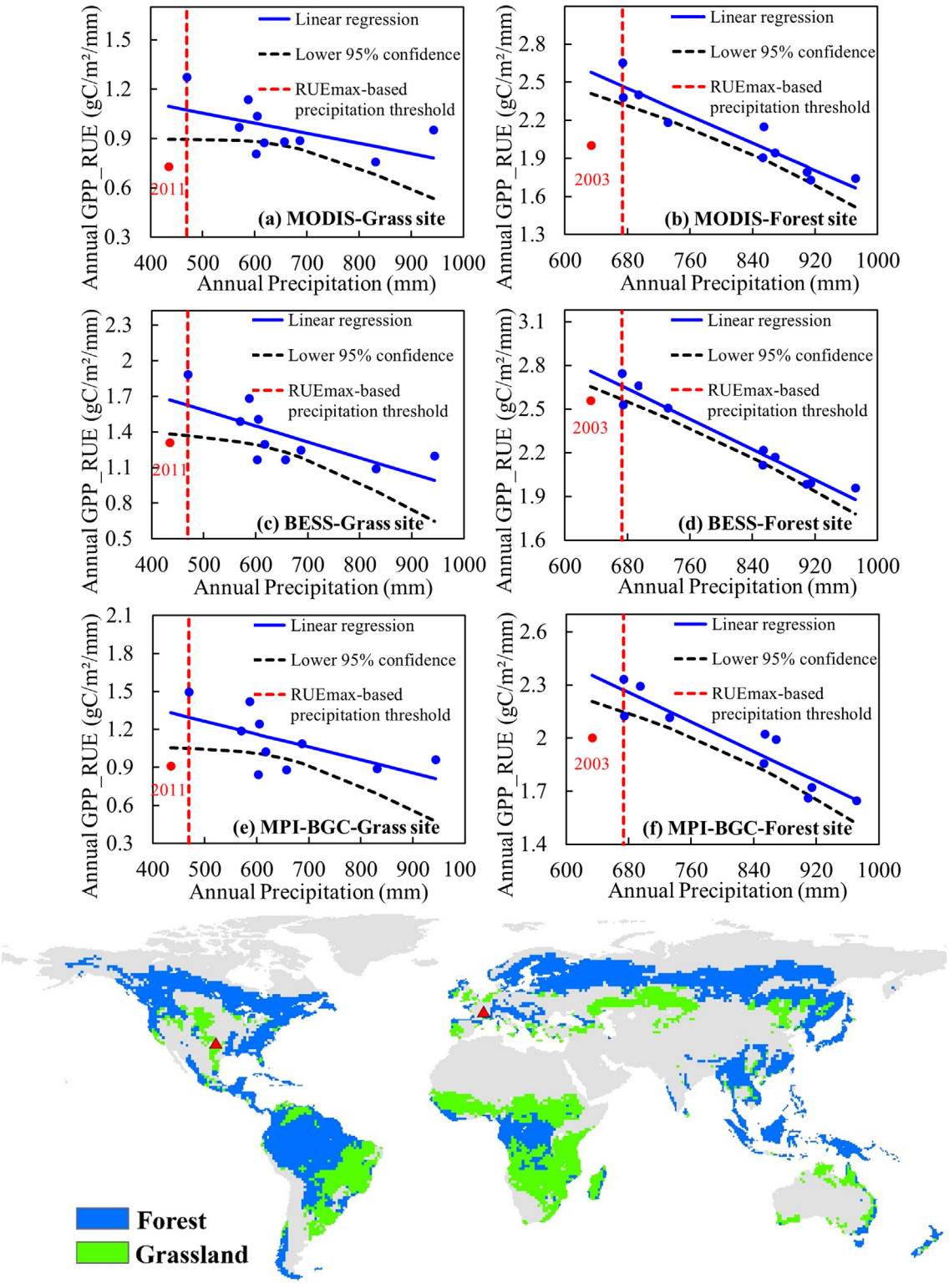

Fig. 1. Examples of ecosystem function loss at a forest site and a grassland site for 2001–2011 using MODIS RUE (a and b), BESS RUE (c and d), and MPI-BGC RUE (e and f) datasets respectively. The forest site was in Europe (3.54° N, 46.48°E) while the grassland site was in southern U.S. (36.23°N, 98.74°W) (Red triangles). The distribution of forest and grassland was based on Commonwealth Scientific and Industrial Research Organisation (CSIRO) vegetation types used by Community Atmosphere Biosphere Land Exchange (CABLE) model. Red dashed lines represent the precipitation threshold based on the maximum of RUE (RUE_{max}), blue solid lines represent the linear regression models built using data points in normal years, black dashed lines represent the lower 95% confidence boundary of the regression, and blue points represent data points in normal years while red points represent data points in possible drought years. The red points that fall below the lower 95% confidence boundary were identified as ecosystem function losses (i.e. data points 2011 and 2003).

variation of the precipitation threshold largely depends on the distribution of land cover types. Tropical forest areas, e.g. the Amazon, have the highest precipitation threshold, which could be >1600 mm/yr. However, the precipitation threshold in semi-arid and arid areas could be as low as 200 mm/yr, e.g. Northwestern China, where shrubland and grassland are largely distributed.

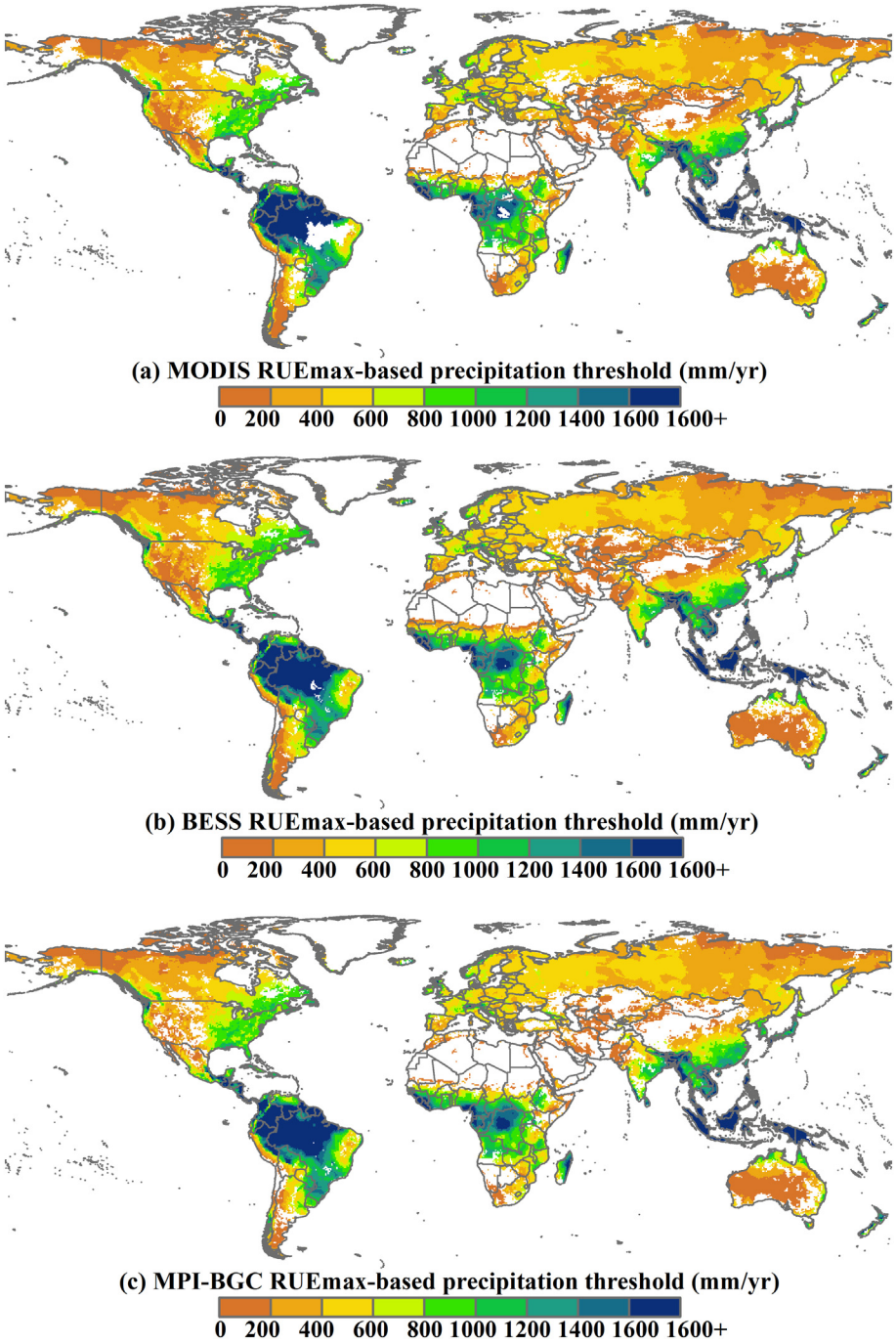

Fig. 2. Spatial distribution of precipitation thresholds based on maximum rain-use efficiency (RUE_{max}) during 2001–2011 using MODIS dataset (a), BESS dataset (b), and MPI-BGC dataset (c). Extreme drought-induced ecosystem function loss is expected to occur if the precipitation in a given year decreases below the threshold on the map.

3.2. Spatial distributions of extreme drought-induced loss of ecosystem function

In this study, annual global distributions of ecosystem function loss due to extreme drought were captured during 2001–2011 based on MODIS, BESS, and MPI-BGC datasets. Additionally, the driest year of ecosystem function loss with the largest deviation from the regression model was also identified in each pixel for each GPP dataset, representing the most extreme loss of ecosystem function (Fig. 3). Large well-known extreme drought events during 2001–2011 were successfully captured in all three RUE datasets (Fig. 3). Extreme drought-induced loss of ecosystem function was mainly concentrated in semi-arid regions. For example, the 2001 seasonal drought in North China (Liu et al., 2014), the prolonged droughts around 2002 in central North America (Michaelian et al., 2011; Schwalm et al., 2012), the 2003 Europe drought induced by heat wave (Ciais et al., 2005), the 2010 drought in Russian (Barriopedro et al., 2011), and the 2011 Southern Great Plains drought in the U.S (Tadesse et al., 2015). In particular, the 2010 Russian drought was identified as the largest ecological response to extreme drought in the study period, which caused approximately 520,000 km^2 of area to lose function on average, over 60% of which was cropland. Based on the global patterns of ecosystem function loss for the period of 2001–2015 (Fig. S3), more recent extreme drought events with ecosystem function loss were also captured, such as the

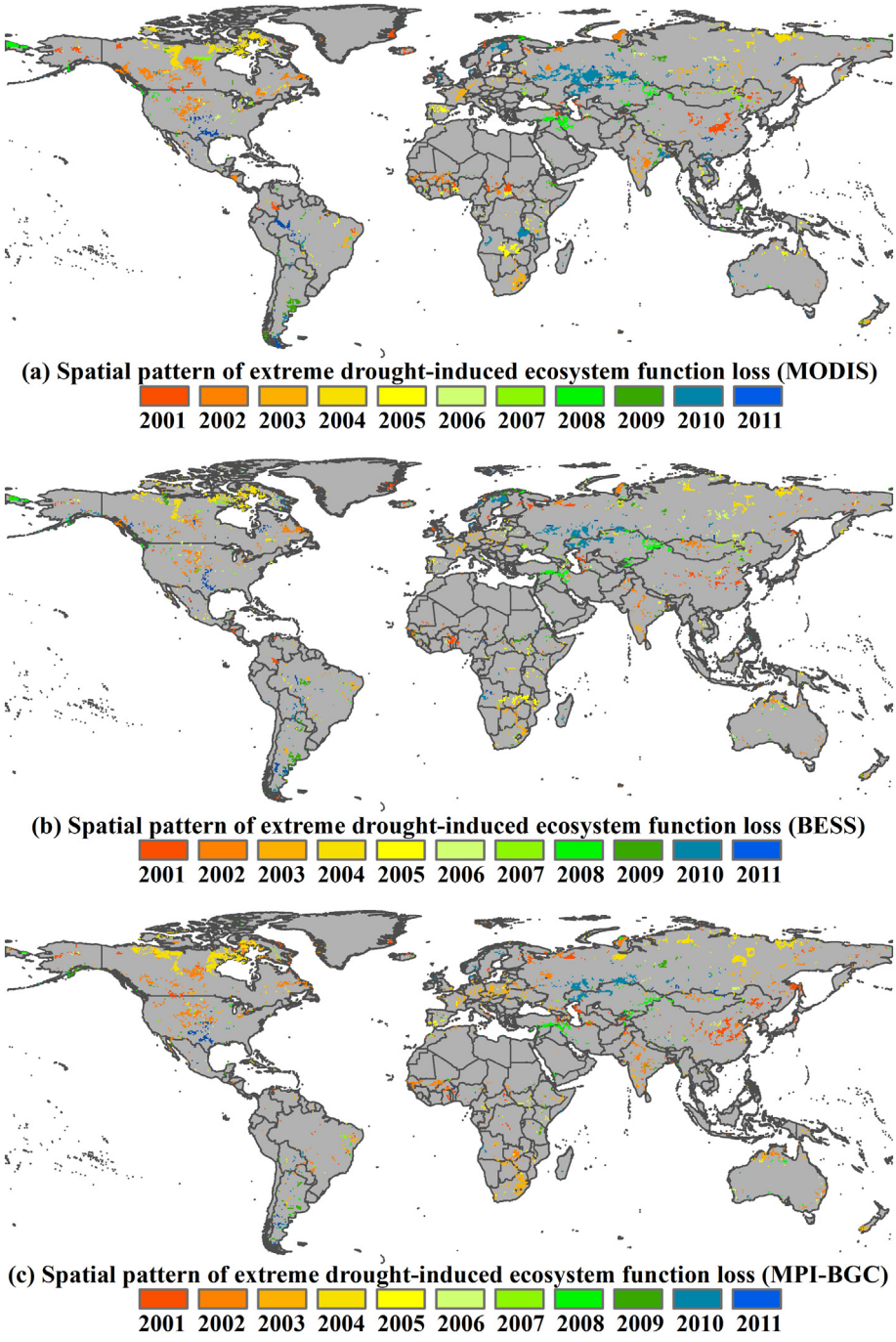

Fig. 3. Spatiotemporal distribution of extreme drought-induced loss of ecosystem function during 2001–2011. Each color on the maps represents the driest year of ecosystem function loss with the largest deviation from the regression model. Extreme droughts in North China (2001), central North America (2002), central Europe (2003), western Russia (2010), and southern U.S. (2011) stand out as exceptional instances of ecosystem function loss in the MODIS (a), BESS (b), and MPI-BGC (c) datasets.

2012 drought in northern central U.S. following the 2011 drought in southern U.S. (http://www.ncdc.noaa.gov/sotc/briefings/201209.pdf), and the 2015 drought in Europe after the 2003 drought (Ionita et al., 2017).

We quantitatively compared the distribution and years of ecosystem function loss in this study with the drought-induced plant mortality events reviewed in (Allen et al., 2010) before 2010 for validation (Table S1). We overlapped 42 forest mortality cases occurred in 1999–2010 from (Allen et al., 2010) with our results (Fig. S4). Specific latitude and longitude information for each mortality case were collected based on references noted in (Allen et al., 2010). For those drought cases without exact latitude and longitude, we located their position by using the specific name of the drought location and Google Earth. Generally, our method matched the extreme droughts very well in Asia (e.g. North China, 2001), Europe (e.g. Central Europe, 2003) and North America (e.g. Central North America, 2002), where the drought year of major ecosystem function loss in this study was within the range of documented years of drought-induced plant mortality events in (Allen et al., 2010) (Table S1). However, in this study, the tropical forest areas did not show much extreme drought signal, e.g. the Amazon drought in 2005 and 2010 were not well detected.

3.3. Spatiotemporal variation of ecosystem function loss and its impact on carbon cycle

In the study period of 2001–2011, extreme drought-induced loss of ecosystem function affected 8% ± 1% of global vegetated land area (9.28 ± 1.33 million km^2), an area roughly the size of China, which resulted in GPP reduction of 1.5 ± 0.3 PgC in total. Here, the vegetated land area estimated in this study was ~120 million km^2. On average, up to 0.9% ± 0.1% of earth's vegetated land (1.13 ± 0.17 million km^2) experienced loss of ecosystem function and 0.14 ± 0.03 PgC GPP was reduced per year. Thus, there was an average decrease in carbon uptake of 120.5 ± 9.9 gC/m^2/yr. In this study, 2002 and 2010 were shown as the major ecological drought years based on the three RUE datasets (Fig. 4a–b), which were mainly attributed to the loss of ecosystem function in central North America (2002) and the droughts in Russia (2010) respectively. In addition, we also analyzed the annual drought-affected area and GPP reduction at the biome level (Fig. 4c–d). Based on the results from the three RUE datasets, cropland and C3 grassland showed relatively high values of affected area and GPP reduction while deciduous needle leaf forest (DNF) and shrubland displayed the lowest values of affected area and GPP reduction.

Ecosystem function loss was distributed mostly in semi-arid regions and exhibited strong interannual variation. We compared the variation in GPP reduction with the variation in GPP anomaly in drought-affected areas (8% ± 1% of vegetated land area). The GPP reductions estimated from the three GPP datasets all showed significant correlation with their GPP anomalies ($R^2 = 0.70–0.91$, $p \leq 0.001$) (Fig. 5). Additionally, the GPP reduction during 2001–2015 based on the average of MODIS GPP and BESS GPP also showed significant correlation with its GPP anomaly in drought-affected areas ($R^2 = 0.60$, $p < 0.001$) (Fig. S5).

4. Discussion

4.1. Advantages and limitations of the method

In this study, the relationship between RUE and precipitation was used to identify the global patterns of extreme drought-induced ecosystem function loss. Based on this, the impacts of ecosystem function loss on carbon uptake were further analyzed. Our detection of losses of ecosystem function was based on the assumption that RUE of an ecosystem increases to a maximum during moderate drought and then declines during extreme drought, which is more ecologically relevant than traditional approaches which rely on meteorological variables and statistical techniques and can further improve our understanding of ecosystem responses to climate extremes (Ciais et al., 2005; Zhao and Running, 2010; Liu et al., 2013; Hoover et al., 2014; Zscheischler et al., 2014). Our results showed that semi-arid regions were hot spots of ecosystem function loss. There was an average decrease in carbon uptake of 120.5 ± 9.9 gC/m^2/yr, which is comparable with multi-year regional averages of drought impact in western America of 116 gC/m^2/yr (Schwalm et al., 2012) and in Europe of 195 gC/m^2/yr (Ciais et al., 2005). The reduced carbon uptake due to ecosystem function loss could strongly influence the regional carbon cycle. The simplicity of the method and integration of an ecological perspective to identify climate extremes are the primary advantages of this study.

In our method, the lower 95% confidence bound of a regression model estimated during normal conditions was used to identify the ecosystem function loss induced by extreme drought, which fits the definition proposed by (Smith, 2011) of "an extreme climatic event is an episode or occurrence in which a statistically rare or unusual climatic period alters ecosystem structure and/or functions well outside the bounds of normal variability" (Smith, 2011). In addition, the exploration

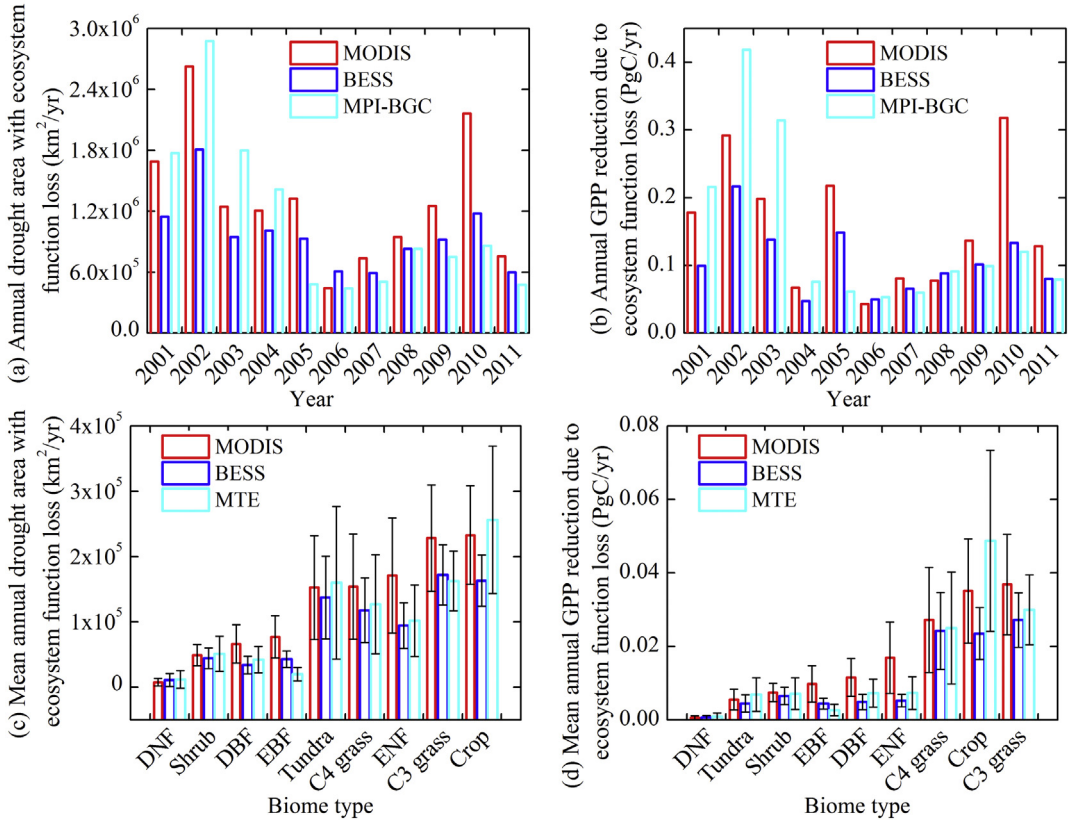

Fig. 4. Mean drought-affected area and GPP reduction caused by ecosystem function loss at annual global scale (a and b) and biome level (c and d) based on three GPP products.

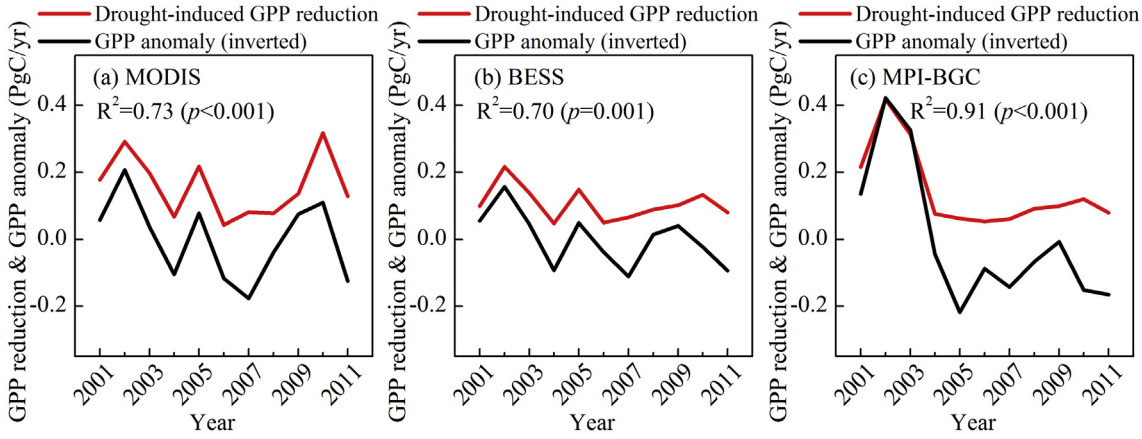

Fig. 5. Interannual variation in GPP reduction (Red lines) and inverted GPP anomaly (Black lines) in drought-affected areas from 2001 to 2011. GPP reductions and anomalies were estimated from MODIS datasets (a), BESS datasets (b), and MPI-BGC datasets (c) respectively. GPP anomaly in each year was calculated as the difference of the GPP value of current year and the average of the study period. R^2 is the determination coefficient which represents the percentage of GPP anomaly explained by reduced carbon uptake due to drought.

of precipitation thresholds provides useful information for the setup of field rainfall manipulation experiments (Fig. 2). For example, at a given location, we provide references for what level of precipitation could be set as the extreme drought condition in a gradient precipitation experiment. While these thresholds are merely starting points with little published literature to compare with, Verbesselt et al. found a threshold for ecosystem collapse in Amazon forests during drought to be 1500 mm/yr, which is comparable with the precipitation threshold identified in our study (>1600 mm/yr) (Verbesselt et al., 2016). Using RUE as a metric of ecosystem function, we were also able to connect the estimates derived from remote sensing and model simulations to field experiments where RUE is most commonly used (Huxman et al., 2004; Yang et al., 2010; Yan et al., 2014).

Significant relationships between RUE and precipitation ($p < 0.05$) were found in >80% of earth's vegetated area, and were further used to analyze ecosystem function loss. Most of the insignificant ($p \geq 0.05$) RUE-precipitation relationships were concentrated in semi-arid regions. Irrigation, which is quite common in semi-arid regions (e.g. Central U.S. and Inner Mongolia, China), could be one of the reasons for insignificant regressions. Also, the accuracy of precipitation data in those regions needs to be improved (Schneider et al., 2013). In this study, short-term, seasonal droughts within a year may not be well detected from the relationship between RUE and precipitation since these variables are estimated at the annual scale. Moreover, in Fig. 1, a spurious pattern could emerge in the correlation between RUE and precipitation if GPP and precipitation were unrelated in this study (Brett, 2004). All global estimates in our results could be conservative due to the limitations in the method and the available analyzed pixels (Fig. S1).

4.2. Well-known extreme drought events in this study

Ecosystem function loss was detected in many well-known extreme drought events, especially in semi-arid areas (e.g. central North America, central Africa, and northwestern China, where cropland and C3 grassland are largely distributed) (Fig. 3). However, for tropical areas, e.g. Amazon forest, we didn't see much extreme drought signal (e.g. 2005 drought or 2010 drought) from any of the three GPP RUE datasets, which could also result in underestimation of ecosystem function loss in this study. Because of the cloudy weather in tropical areas, optical remote sensing images usually have low quality, which may impact the quality of GPP derived from remote sensing (Anav et al., 2015). For the up-scaled GPP from FLUXNET, due to the few flux towers located in tropical forests, high error exists in the GPP estimates (Kumar et al., 2016). Additionally, process model-based GPP simulations in tropical areas still remains a challenge due to the uncertainty caused by climatic forcing data (Wu et al., 2017). In this study, tundra areas also showed a strong signal of ecosystem function loss, especially in 2004 (Fig. 3). Due to large amounts of peatland distributed in tundra, fire frequently occurs in the dry season (Mack et al., 2011). The high carbon content of the peatland may largely contribute to the fire occurrence in association with extreme drought (Turetsky et al., 2014). In this study, those fire occurrences were recognized as ecosystem function loss due to extreme droughts, as drought likely initiated higher fire probability. For cropland, human management also has strong influence on the production of plants (i.e. harvest) and may thus influence drought detection. However, we didn't remove the cropland in this study. Usually, at a cropland site, the timing of seeding, growing and harvesting remains the same, thus the GPP estimates of this site are still comparable at the annual scale.

4.3. Implication of ecosystem function loss on carbon cycle

In this study, semi-arid regions were shown to be hot spots of ecosystem function loss, and contributed to >70% of the annual GPP variation in drought-affected areas (Fig. 5). However, the extreme drought-induced ecosystem function loss was found to have little impact on global GPP variability. In semi-arid regions, GPP variability is strongly controlled by precipitation variability, which could be one of the reasons that local ecosystems are more predisposed to loss of ecosystem function. Also, studies have shown that the productivity in semi-arid regions strongly contributes to the interannual variability of global GPP or NPP (Huang et al., 2016; Zhang et al., 2016). In our results, even though 0.14 ± 0.03 PgC/yr GPP reduction due to ecosystem functional loss didn't show a strong impact on the global carbon cycle (results not shown), it was still a major threat at the regional scale and could potentially influence the global carbon cycle. No increasing trend of GPP reduction was found in this study, and there was even a decreasing trend in ecosystem function loss from 2001 to 2015 (Fig. S5). The continually increasing atmospheric CO_2 concentration may stimulate higher water-use efficiency of ecosystems despite the warming during the period (Keenan et al., 2013). However, as ecosystem function loss still largely depends on the climate variability, considering the increasing precipitation variability and expansion of dry land (Huang et al., 2015), extreme drought-induced ecosystem function loss may have a larger effect on the future of regional and global carbon cycles.

5. Conclusions

Quantifying the ecological patterns of extreme drought-induced ecosystem function loss is an important first step to understand how ecosystems respond to ecological drought against the background of climate change. Here, we developed a novel method based on plant community rain-use efficiency to detect ecosystem function loss globally. We produced spatial patterns of extreme drought-induced ecosystem function loss during 2001–2011 based on three different GPP products. Large well-known extreme drought events with ecosystem function loss were well captured in semi-arid regions. Extreme drought-induced loss of ecosystem function could explain >70% of the GPP variability in drought-affected areas. Our study demonstrates the importance of semi-arid regions in terrestrial carbon cycle studies and provides a new simple way to quantify extreme droughts from the ecological perspective.

Acknowledgments

Funding for this study was provided by US Department of Energy grants DE-SC00114085, and US National Science Foundation (NSF) grants EF 1137293 and OIA-1301789. This work extends previous research detailed in a MS thesis by N. Mikle (Thesis title: A global assessment of drought-induced losses of ecosystem function, University of Oklahoma, 2014).

Appendix A. Supplementary data

Supplementary data to this article can be found online at https://doi.org/10.1016/j.scitotenv.2018.02.114.

References

Allen, C.D., et al., 2010. A global overview of drought and heat-induced tree mortality reveals emerging climate change risks for forests. For. Ecol. Manag. 259 (4):660–684. https://doi.org/10.1016/j.foreco.2009.09.001.

Anav, A., et al., 2015. Spatiotemporal patterns of terrestrial gross primary production: a review. Rev. Geophys. 53 (3):785–818. https://doi.org/10.1002/2015rg000483.

Barriopedro, D., Fischer, E.M., Luterbacher, J., Trigo, R., Garcia-Herrera, R., 2011. The hot summer of 2010: redrawing the temperature record map of Europe. Science 332 (6026):220–224. https://doi.org/10.1126/science.1201224.

Breshears, D.D., et al., 2005. Regional vegetation die-off in response to global-change-type drought. Proc. Natl. Acad. Sci. U. S. A. 102 (42):15144–15148. https://doi.org/10.1073/pnas.0505734102.

Brett, M.T., 2004. When is a correlation between non-independent variables "spurious"? Oikos 105 (3):647–656. https://doi.org/10.1111/j.0030-1299.2004.12777.x.

Choat, B., et al., 2012. Global convergence in the vulnerability of forests to drought. Nature 491 (7426):752–755. https://doi.org/10.1038/nature11688.

Ciais, P., et al., 2005. Europe-wide reduction in primary productivity caused by the heat and drought in 2003. Nature 437 (7058):529–533. https://doi.org/10.1038/nature03972.

Doughty, C.E., et al., 2015. Drought impact on forest carbon dynamics and fluxes in Amazonia. Nature 519 (7541):78–82. https://doi.org/10.1038/nature14213.

Estiarte, M., et al., 2016. Few multiyear precipitation-reduction experiments find a shift in the productivity-precipitation relationship. Glob. Chang. Biol. 22 (7):2570–2581. https://doi.org/10.1111/gcb.13269.

Frank, D., et al., 2015. Effects of climate extremes on the terrestrial carbon cycle: concepts, processes and potential future impacts. Glob. Chang. Biol. 21 (8):2861–2880. https://doi.org/10.1111/gcb.12916.

Harris, I., Jones, P.D., Osborn, T.J., Lister, D.H., 2014. Updated high-resolution grids of monthly climatic observations — the CRU TS3.10 dataset. Int. J. Climatol. 34 (3): 623–642. https://doi.org/10.1002/joc.3711.

Hoover, D.L., Knapp, A.K., Smith, M.D., 2014. Resistance and resilience of a grassland ecosystem to climate extremes. Ecology 95 (9):2646–2656. https://doi.org/10.1890/13-2186.1.

Huang, J., Yu, H., Guan, X., Wang, G., Guo, R., 2015. Accelerated dryland expansion under climate change. Nat. Clim. Chang. https://doi.org/10.1038/nclimate2837.

Huang, L., He, B., Chen, A., Wang, H., Liu, J., Lu, A., Chen, Z., 2016. Drought dominates the interannual variability in global terrestrial net primary production by controlling semi-arid ecosystems. Sci. Rep. 6, 24639. https://doi.org/10.1038/srep24639.

Huxman, T.E., Smith, M.D., Fay, P.A., 2004. Convergence across biomes to a common rain-use efficiency. Nature 429 (6992):651–654. https://doi.org/10.1038/nature02597.

Ionita, M., Tallaksen, L.M., Kingston, D.G., Stagge, J.H., Laaha, G., Van Lanen, H.A.J., Scholz, P., Chelcea, S.M., Haslinger, K., 2017. The European 2015 drought from a climatological perspective. Hydrol. Earth Syst. Sci. 21 (3):1397–1419. https://doi.org/10.5194/hess-21-1397-2017.

Jentsch, A., et al., 2011. Climate extremes initiate ecosystem-regulating functions while maintaining productivity. J. Ecol. 99 (3):689–702. https://doi.org/10.1111/j.1365-2745.2011.01817.x.

Jiang, C., Ryu, Y., 2016. Multi-scale evaluation of global gross primary productivity and evapotranspiration products derived from breathing earth system simulator (BESS). Remote Sens. Environ. 186:528–547. https://doi.org/10.1016/j.rse.2016.08.030.

de Jong, R., Schaepman, M.E., Furrer, R., de Bruin, S., Verburg, P.H., 2013. Spatial relationship between climatologies and changes in global vegetation activity. Glob. Chang. Biol. 19 (6):1953–1964. https://doi.org/10.1111/gcb.12193.

Jung, M., et al., 2011. Global patterns of land-atmosphere fluxes of carbon dioxide, latent heat, and sensible heat derived from eddy covariance, satellite, and meteorological observations. J. Geophys. Res. 116. https://doi.org/10.1029/2010jg001566.

Keenan, T.F., Hollinger, D.Y., Bohrer, G., Dragoni, D., Munger, J.W., Schmid, H.P., Richardson, A.D., 2013. Increase in forest water-use efficiency as atmospheric carbon dioxide concentrations rise. Nature 499 (7458):324–327. https://doi.org/10.1038/nature12291.

Knapp, A.K., Ciais, P., Smith, M.D., 2017. Reconciling inconsistencies in precipitation-productivity relationships: implications for climate change. New Phytol. 214 (1): 41–47. https://doi.org/10.1111/nph.14381.

Kumar, J., Hoffman, F.M., Hargrove, W.W., Collier, N., 2016. Understanding the representativeness of FLUXNET for upscaling carbon flux from eddy covariance measurements. Earth System Science Data Discussions:1–25 https://doi.org/10.5194/essd-2016-36.

Liu, G., Liu, H., Yin, Y., 2013. Global patterns of NDVI-indicated vegetation extremes and their sensitivity to climate extremes. Environ. Res. Lett. 8 (2), 025009. https://doi.org/10.1088/1748-9326/8/2/025009.

Liu, Y., Zhou, Y., Ju, W., Wang, S., Wu, X., He, M., Zhu, G., 2014. Impacts of droughts on carbon sequestration by China's terrestrial ecosystems from 2000 to 2011. Biogeosciences 11 (10):2583–2599. https://doi.org/10.5194/bg-11-2583-2014.

Luo, Y.Q., Jiang, L.F., Niu, S.L., Zhou, X.H., 2017. Nonlinear responses of land ecosystems to variation in precipitation. New Phytol. 214 (1):5–7. https://doi.org/10.1111/nph.14476.

Mack, M.C., Bret-Harte, M.S., Hollingsworth, T.N., Jandt, R.R., Schuur, E.A.G., Shaver, G.R., Verbyla, D.L., 2011. Carbon loss from an unprecedented Arctic tundra wildfire. Nature 475 (7357):489–492. https://doi.org/10.1038/nature10283.

Mariotte, P., Vandenberghe, C., Kardol, P., Hagedorn, F., Buttler, A., Schwinning, S., 2013. Subordinate plant species enhance community resistance against drought in semi-natural grasslands. J. Ecol. 101 (3):763–773. https://doi.org/10.1111/1365-2745.12064.

McDowell, N., et al., 2008. Mechanisms of plant survival and mortality during drought: why do some plants survive while others succumb to drought? New Phytol. 178 (4):719–739. https://doi.org/10.1111/j.1469-8137.2008.02436.x.

Michaelian, M., Hogg, E.H., Hall, R.J., Arsenault, E., 2011. Massive mortality of aspen following severe drought along the southern edge of the Canadian boreal forest. Glob. Chang. Biol. 17 (6):2084–2094. https://doi.org/10.1111/j.1365-2486.2010.02357.x.

Peng, C.H., Ma, Z.H., Lei, X.D., Zhu, Q., Chen, H., Wang, W.F., Liu, S.R., Li, W.Z., Fang, X.Q., Zhou, X.L., 2011. A drought-induced pervasive increase in tree mortality across Canada's boreal forests. Nat. Clim. Chang. 1 (9):467–471. https://doi.org/10.1038/Nclimate1293.

Piao, S., et al., 2013. Evaluation of terrestrial carbon cycle models for their response to climate variability and to CO_2 trends. Glob. Chang. Biol. 19 (7):2117–2132. https://doi.org/10.1111/gcb.12187.

Ponce Campos, G.E., et al., 2013. Ecosystem resilience despite large-scale altered hydroclimatic conditions. Nature 494 (7437):349–352. https://doi.org/10.1038/nature11836.

Reichstein, M., et al., 2013. Climate extremes and the carbon cycle. Nature 500 (7462): 287–295. https://doi.org/10.1038/nature12350.

Reyer, C.P., et al., 2013. A plant's perspective of extremes: terrestrial plant responses to changing climatic variability. Glob. Chang. Biol. 19 (1):75–89. https://doi.org/10.1111/gcb.12023.

Schneider, U., Becker, A., Finger, P., Meyer-Christoffer, A., Ziese, M., Rudolf, B., 2013. GPCC's new land surface precipitation climatology based on quality-controlled in situ data and its role in quantifying the global water cycle. Theor. Appl. Climatol. 115 (1–2): 15–40. https://doi.org/10.1007/s00704-013-0860-x.

Schwalm, C.R., Williams, C.A., Schaefer, K., Baldocchi, D., Black, T.A., Goldstein, A.H., Law, B. E., Oechel, W.C., Paw U, K.T., Scott, R.L., 2012. Reduction in carbon uptake during turn of the century drought in western North America. Nat. Geosci. 5 (8):551–556. https://doi.org/10.1038/ngeo1529.

Smith, M.D., 2011. An ecological perspective on extreme climatic events: a synthetic definition and framework to guide future research. J. Ecol. 99 (3):656–663. https://doi.org/10.1111/j.1365-2745.2011.01798.x.

Stocker, T.F., Qin, D., Plattner, G., Tignor, M., Allen, S., Boschung, J., Nauels, A., Xia, Y., Bex, V., Midgley, P., 2013. Climate change 2013: the physical science basis. Intergovernmental Panel on climate Change, Working Group I contribution to the IPCC Fifth Assessment Report (AR5). C. U. Press, New York.

Tadesse, T., Wardlow, B.D., Brown, J.F., Svoboda, M.D., Hayes, M.J., Fuchs, B., Gutzmer, D., 2015. Assessing the vegetation condition impacts of the 2011 drought across the U. S. Southern Great Plains using the vegetation drought response index (VegDRI). J. Appl. Meteorol. Climatol. 54 (1):153–169. https://doi.org/10.1175/jamc-d-14-0048.1.

Turetsky, M.R., Benscoter, B., Page, S., Rein, G., van der Werf, G.R., Watts, A., 2014. Global vulnerability of peatlands to fire and carbon loss. Nat. Geosci. 8 (1):11–14. https://doi.org/10.1038/ngeo2325.

Verbesselt, J., Umlauf, N., Hirota, M., Holmgren, M., Van Nes, E.H., Herold, M., Zeileis, A., Scheffer, M., 2016. Remotely sensed resilience of tropical forests. Nat. Clim. Chang. 6 (11):1028–1031. https://doi.org/10.1038/nclimate3108.

Wu, D., Zhao, X., Liang, S., Zhou, T., Huang, K., Tang, B., Zhao, W., 2015. Time-lag effects of global vegetation responses to climate change. Glob. Chang. Biol. 21 (9):3520–3531. https://doi.org/10.1111/gcb.12945.

Wu, Z., Ahlstroem, A., Smith, B., Ardo, J., Eklundh, L., Fensholt, R., Lehsten, V., 2017. Climate data induced uncertainty in model based estimations of terrestrial primary productivity. Environ. Res. Lett. https://doi.org/10.1088/1748-9326/aa6fd8.

Yan, L., Luo, Y., Sherry, R.A., Bell, J.E., Zhou, X., Xia, J., 2014. Rain use efficiency as affected by climate warming and biofuel harvest: results from a 12-year field experiment. GCB Bioenergy 6 (5):556–565. https://doi.org/10.1111/gcbb.12081.

Yang, Y.H., Fang, J.Y., Fay, P.A., Bell, J.E., Ji, C.J., 2010. Rain use efficiency across a precipitation gradient on the Tibetan Plateau. Geophys. Res. Lett. 37 (doi: Artn L15702 10.1029/2010gl043920).

Zhang, Y., et al., 2016. Precipitation and carbon-water coupling jointly control the interannual variability of global land gross primary production. Sci. Rep. 6, 39748. https://doi.org/10.1038/srep39748.

Zhao, M., Running, S.W., 2010. Drought-induced reduction in global terrestrial net primary production from 2000 through 2009. Science 329 (5994):940–943. https://doi.org/10.1126/science.1192666.

Zscheischler, J., et al., 2014. A few extreme events dominate global interannual variability in gross primary production. Environ. Res. Lett. 9 (3), 035001. https://doi.org/10.1088/1748-9326/9/3/035001.